nature chemical biology

ARTICLES

https://doi.org/10.1038/s41589-020-00668-4

Peroxisome compartmentalization of a toxic enzyme improves alkaloid production

Parbir S. Grewal[1,7], Jennifer A. Samson[2,5,7], Jordan J. Baker[2,3], Brian Choi[1,6] and John E. Dueber[2,4] ✉

Eukaryotic cells compartmentalize metabolic pathways in organelles to achieve optimal reaction conditions and avoid crosstalk with cytosolic factors. We found that cytosolic expression of norcoclaurine synthase (NCS), the enzyme that catalyzes the first committed reaction in benzylisoquinoline alkaloid biosynthesis, is toxic in *Saccharomyces cerevisiae* and, consequently, restricts (*S*)-reticuline production. We developed a compartmentalization strategy that alleviates NCS toxicity while promoting increased (*S*)-reticuline titer. This strategy is achieved through efficient targeting of toxic NCS to the peroxisome while, crucially, taking advantage of the free flow of metabolite substrates and products across the peroxisome membrane. We demonstrate that expression of engineered transcription factors can mimic the oleate response for larger peroxisomes, further increasing benzylisoquinoline alkaloid titer without the requirement for peroxisome induction with fatty acids. This work specifically addresses the challenges associated with toxic NCS expression and, more broadly, highlights the potential for engineering organelles with desired characteristics for metabolic engineering.

Cell factories, using production hosts including bacterial, fungal, mammalian and plant cells, are used to make important industrial products, including pharmaceuticals, proteins, commodity chemicals and biofuels[1–4]. As cellular engineering becomes increasingly sophisticated, incorporating longer and more complex heterologous metabolic pathways, the likelihood of crosstalk with native cellular functions in the host cell also increases. Consequently, there is greater risk for cytotoxicity and effects on host cell growth. Reduced growth has many negative consequences, including reductions in product titer due to fewer cells, decreases in production rate due to slower growth and decreases in strain robustness because mutations that relieve toxicity are often ones that reduce or eliminate pathway flux.

Subcellular compartmentalization is an evolved strategy for coping with unproductive or harmful crosstalk[5,6]. In eukaryotes, lipid membrane-enclosed organelles are used to direct enzymatic activity toward specific substrates. For example, vacuolar proteases have broad substrate specificity, but their degradative activity is directed toward only vacuolar targets due to compartmentalization[7]. Compartments are also used to sequester toxic metabolites. The parasite *Trypanosoma brucei*, during the part of its life cycle in the human bloodstream, respecializes peroxisomes from organelles that perform the β-oxidation of fatty acids to organelles called glycosomes where the early steps of glycolysis are compartmentalized. While most organisms use allosteric feedback regulation of these glycolytic enzymes to prevent toxic accumulation of intermediates, *T. brucei* instead uses a compartmentalization strategy to enable increased flux while preventing toxic intermediate accumulation in the cytosol[8]. In biomanufacturing, compartmentalization may prove to be a powerful strategy to isolate toxic heterologous components away from the host cell cytosol, thereby limiting cytotoxicity, improving growth and increasing product titer.

We discovered that a titer-limiting enzyme in the industrially valued benzylisoquinoline alkaloid (BIA) family of plant natural products is toxic when expressed in a yeast production host. The BIA family consists of ~2,500 natural products exhibiting a variety of therapeutic bioactivities, including antibacterial (berberine, sanguinarine), anticancer (noscapine), antispasmodic (papaverine) and analgesic (codeine, morphine) activities[9]. The first committed BIA molecule, (*S*)-norcoclaurine (**5**), is produced through the condensation of two tyrosine-derived substrates, dopamine (**4**) and 4-hydroxyphenylacetaldehyde (4-HPAA; **3**), by the enzyme NCS (Fig. 1a)[9]. NCS is thought to be a gatekeeper enzyme that restricts entry into the BIA pathway[10]. Accordingly, high NCS activity is required for high production levels of BIAs in heterologous hosts. However, we found that our most active variant of NCS was toxic when expressed in the cytosol of *S. cerevisiae*. Although the mechanism of toxicity is unknown, we determined that toxicity is unrelated to (*S*)-norcoclaurine biosynthesis and hypothesize that it is caused by interactions between NCS and a native yeast factor.

We propose repurposing the yeast peroxisome as the site for subcellular compartmentalization of toxic NCS. The peroxisome has several attributes that make it an attractive compartment for alleviating NCS toxicity without inhibiting flux through the BIA pathway. First, peroxisomes are not essential for *S. cerevisiae* viability under typical glucose-based fermentation conditions, so they can be repurposed without detriment to the cell[11]. Second, heterologous protein can be targeted to the peroxisome by simply appending a small peptide tag (peroxisomal targeting signal type 1, PTS1)[12] to the C terminus of the protein of interest. Third, the peroxisome is thought to contain the highest concentration of protein in the eukaryotic cell[13,14] and can compartmentalize an impressive amount of heterologous cargo[11], more than has been demonstrated for other organelles[15]. Fourth, peroxisomes are permeable to many small molecules with molecular weight under approximately 500–700 Da,

[1]Department of Chemical & Biomolecular Engineering, University of California, Berkeley, CA, USA. [2]Department of Bioengineering, University of California, Berkeley, CA, USA. [3]UC Berkeley and UCSF Graduate Program in Bioengineering, University of California, Berkeley, CA, USA. [4]Biological Systems & Engineering Division, Lawrence Berkeley National Laboratory, Berkeley, CA, USA. [5]Present address: Sound Agriculture, Emeryville, CA, USA. [6]Present address: Department of Chemical and Biological Engineering, Princeton University, Princeton, NJ, USA. [7]These authors contributed equally: Parbir S. Grewal, Jennifer A. Samson. ✉e-mail: jdueber@berkeley.edu

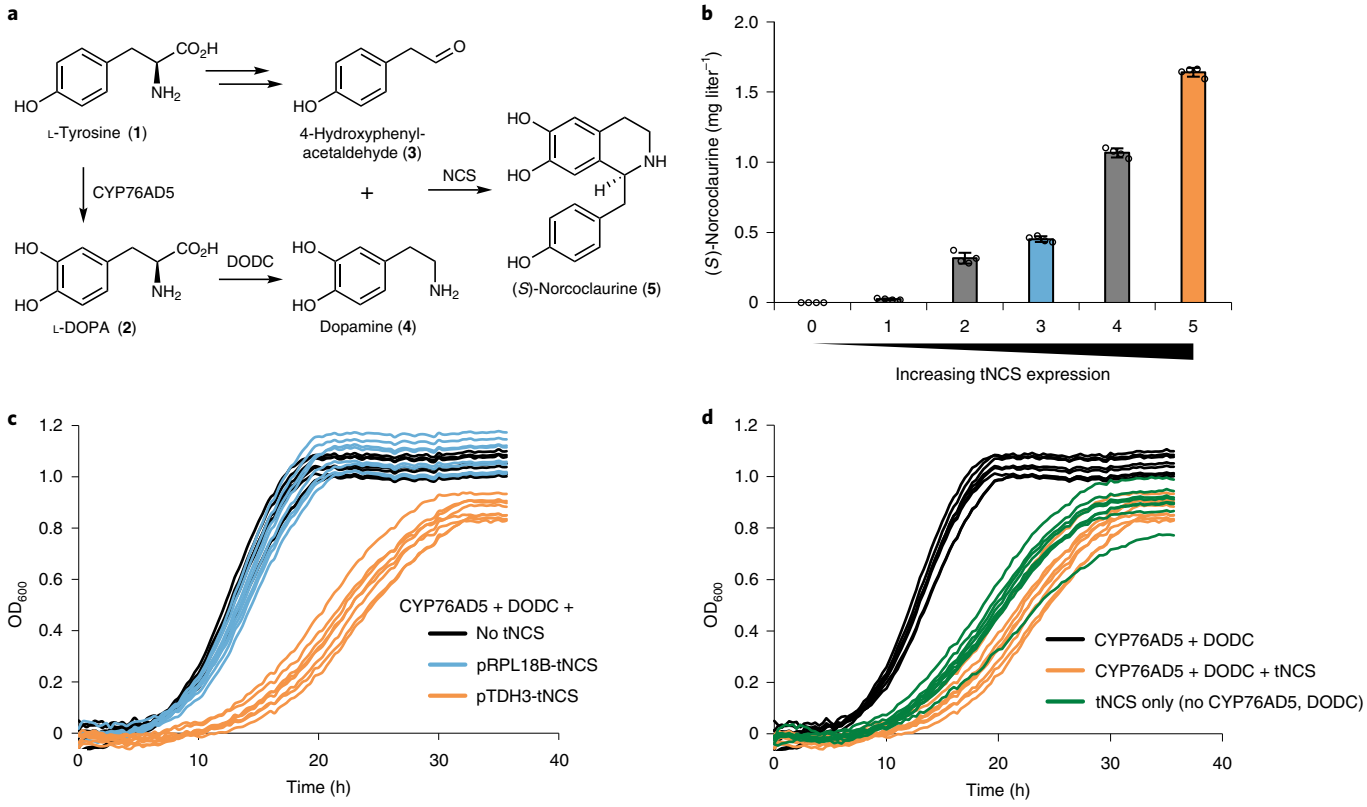

Fig. 1 | Cytosolic expression of tNCS is toxic to *S. cerevisiae*. a, Metabolic pathway for production of (*S*)-norcoclaurine (**5**) from L-tyrosine (**1**) using three heterologous enzymes: CYP76AD5, DODC and tNCS. 4-Hydroxyphenylacetaldehyde (**3**) is produced endogenously by *S. cerevisiae*. **b**, Higher expression of tNCS results in a higher titer of (*S*)-norcoclaurine. The following well-characterized promoters were used to drive expression of tNCS on a CEN6/ARS4 plasmid: 1, pREV; 2, pRNR2; 3, pRPL18B; 4, pTEF1; 5, pTDH3. 0 corresponds to no NCS. Data are shown as the mean ± s.d. of four biological replicates. **c**, Higher expression of tNCS results in slower growth, and toxicity is observed under strong expression by pTDH3. $n = 8$ biological replicates per strain. **d**, Considerable toxicity is observed even in the absence of the enzymes required for dopamine production, CYP76AD5 and DODC (green lines). $n = 8$ biological replicates per strain.

meaning that peroxisomally compartmentalized NCS would likely retain access to its substrates[11,16].

In this study, we demonstrate that compartmentalization of toxic NCS in the peroxisome can alleviate cytotoxicity and improve product titer. We utilize this compartment to selectively partition the toxic enzyme from cytosolic factors while leveraging the ability of the peroxisome to allow small molecule substrates and products to diffuse into and out of the peroxisome lumen. Compartmentalization of toxic NCS enzyme improves production of (*S*)-norcoclaurine and the key branch-point intermediate (*S*)-reticuline. More broadly, we provide a demonstration of the utility of the peroxisome as a two-way insulating compartment, one that can protect the host cell from toxicity associated with heterologous protein and, conversely, can protect heterologous protein from native cellular processes such as degradation. Although the peroxisome naturally has an impressive cargo capacity compared to other organelles, improved capacity is desired for engineering applications. We demonstrate initial progress toward this goal by using engineered transcription factors to mimic peroxisome proliferation that is induced by fatty acids and thereby further improve BIA titer.

Results

Expression of NCS variant causes cytotoxicity in yeast. While connecting yeast central metabolism to the heterologous BIA pathway, we identified the NCS enzyme as a key rate-limiting step preventing high-titer production of BIAs (Fig. 1a)[17]. Several NCS homologs were screened to identify the homolog with the highest activity in yeast. In comparison to our original NCS from *Papaver somniferum*, heterologous expression of the NCS from *Coptis japonica* resulted in threefold higher (*S*)-norcoclaurine titer (Extended Data Fig. 1). Truncation of the N terminus of the *C. japonica* homolog to remove residues upstream of the Bet v1 domain, the critical fold of NCS proteins[9], resulted in a 20-fold-higher titer than with our original *P. somniferum* variant, corresponding to the highest activity described in *S. cerevisiae*. For simplicity, we refer to this truncated *C. japonica* enzyme as tNCS. Previous studies have also reported improved titers upon truncation of NCS enzymes, and evidence suggests that this effect is due to improved protein expression[18–20].

(*S*)-Norcoclaurine titer was directly dependent on the expression level of tNCS, and stronger promoters and higher copy numbers resulted in higher (*S*)-norcoclaurine titers (Fig. 1b). Copy number was increased compared to chromosomal integration by using a CEN6/ARS4 plasmid (~2–5 copies per cell[21]). Transcription levels were controlled using a range of previously characterized yeast promoters[22,23]. Unexpectedly, we observed that expression of tNCS decreased the yeast growth rate in an expression-level-dependent manner (Fig. 1c). Moderate expression of tNCS (pRPL18B promoter) had almost no effect on growth when compared with cells that did not express tNCS, whereas strong expression (pTDH3 promoter) considerably decreased the growth rate and final cell density of the yeast culture.

Expression of tNCS in the cytosol resulted in toxicity, yet the source of toxicity was unclear. To determine whether toxicity results from BIA pathway intermediates, we compared the expression of

tNCS with and without the upstream BIA pathway. Without the upstream enzymes tyrosine hydroxylase (CYP76AD5) and DOPA decarboxylase (DODC), yeast cannot produce dopamine, which is one of two substrates required for (*S*)-norcoclaurine biosynthesis. Even without the upstream pathway, the strain exhibited a reduced growth rate, indicating that toxicity is not due to excessively high levels of (*S*)-norcoclaurine nor is it due to the reaction between dopamine and 4-HPAA (Fig. 1d). Additionally, we fed dopamine and (*S*)-norcoclaurine to the dopamine-producing strain and did not observe toxicity even up to 100 mg liter^{-1} (*S*)-norcoclaurine (Extended Data Fig. 2). We conclude that toxicity is not caused by (*S*)-norcoclaurine biosynthesis but rather is due to some other effect of tNCS. Toxicity could result from an off-target enzyme-catalyzed reaction consuming an essential metabolite or producing a toxic metabolite. However, although NCS enzymes are promiscuous for the aldehyde substrate, they are highly specific for the amine substrate and are only capable of accepting dopamine or closely related molecular analogs[20,24,25], none of which are produced by *S. cerevisiae*[17,26]. Therefore, we hypothesize that tNCS toxicity is caused by an interaction with an unknown yeast factor.

tNCS peroxisome compartmentalization improves BIA titer. Although the mechanism of tNCS toxicity is unknown, we hypothesized that we could alleviate toxicity via subcellular compartmentalization of the tNCS protein. An ideal compartment would sequester toxic tNCS away from the cytosol while allowing diffusion of the enzyme's substrates and products into and out of the compartment. The peroxisome was identified as a promising candidate because it can import fully folded proteins[27], has a high capacity for heterologous protein[11,15], is permeable to small molecules[11,16] and compartmentalization of engineered protein inside the peroxisome should not have adverse effects on yeast viability[11]. Previous work on peroxisomes in vitro[16], and our experiments in vivo[11], have indicated a size exclusion threshold of 500–700 Da on the basis of the permeability of substrates with different molecular weights. The permeability of small molecules across the peroxisome membrane is also affected by the molecule's shape or 'bulkiness', including its hydrodynamic radius[11,16]. We predicted that the dopamine and 4-HPAA substrates, as well as the (*S*)-norcoclaurine product, would be able to cross the peroxisomal membrane given their structure and small molecular weight (153, 136 and 271 Da, respectively). Therefore, if tNCS were compartmentalized inside the peroxisome, it would retain access to its substrates while the (*S*)-norcoclaurine product would diffuse out from the peroxisome to the cytosol (Fig. 2a).

Toxic tNCS was targeted to the peroxisome lumen using a previously engineered C-terminal enhanced PTS1 (ePTS1) and fused with yellow fluorescent protein (YFP) to generate tNCS–YFP–ePTS1. A fluorescent peroxisomal marker consisting of the N terminus of the peroxisomal membrane protein Pex22 fused to red fluorescent protein (RFP) was coexpressed[28]. Colocalization microscopy analysis of RFP and YFP signals demonstrated that ePTS1 can facilitate effective peroxisomal targeting of tNCS (Fig. 2b).

As an orthogonal assessment of peroxisomal compartmentalization, we applied a pigment-producing enzyme sequestration assay to tNCS as previously described[11]. Briefly, the prodeoxyviolacein (PDV) pigment-producing enzyme VioE was fused to tNCS, with the upstream enzymes VioA and VioB expressed in the cytosol. The IPA imine dimer substrate for VioE has low permeability across the peroxisome membrane (Fig. 2a)[11]. Accordingly, fusions between proteins of interest and VioE–ePTS1 can provide an assessment of targeting efficiency for these tagged proteins because better compartmentalized proteins will result in yeast cultures with lower PDV pigment production. As a control, we tagged tNCS–VioE with dead_ePTS1, where the C-terminal leucine is mutated to threonine, resulting in a tag with low affinity for the cargo carrier Pex5p and, therefore, preventing peroxisomal import[11]. tNCS constructs were expressed from a plasmid with a CEN6/ARS4 replication origin and the strong pTDH3 promoter. By visually comparing PDV pigment levels for peroxisomally targeted tNCS fused to VioE (tNCS–VioE–ePTS1) with the levels observed with cytosolic expression (tNCS–VioE–dead_ePTS1), we showed that ePTS1 provides considerable compartmentalization of tNCS at this expression level (Fig. 2c). PDV was quantified by extraction from liquid culture after 3 d of growth, and cells with tNCS–VioE targeted to the peroxisome showed a 40% reduction in PDV pigment relative to those with cytosolic tNCS–VioE.

Host growth and (*S*)-norcoclaurine titer were improved when toxic tNCS was compartmentalized in the peroxisome. In addition to the violacein pathway, our strains contained the upstream BIA pathway (CYP76AD5, DODC) so that (*S*)-norcoclaurine could be directly measured from the same strains. The strain with peroxisomally targeted tNCS achieved a higher final optical density (OD) and growth rate (0.103 versus 0.058 h^{-1}) than the strain where tNCS was cytosolically expressed in growth experiments in microwell plates (Fig. 2d). In fact, the peroxisomally targeted tNCS–VioE–ePTS1 strain grew nearly as well as two control strains lacking toxic tNCS, the VioE–ePTS1 (growth rate 0.136 h^{-1}) and VioE–dead_ePTS1 (growth rate 0.129 h^{-1}) strains. Encouraged by these results, we conducted shake flask fermentations to compare the cell growth and (*S*)-norcoclaurine titer of strains expressing tNCS–VioE–ePTS1 and tNCS–VioE–dead_ePTS1. In addition to a growth improvement as observed in the microwell experiment (Extended Data Fig. 3), we observed a 54% increase in titer and a 2.2-fold increase in maximum productivity (0.13 versus 0.06 mg liter^{-1} per hour) (Fig. 2e).

To demonstrate that the (*S*)-norcoclaurine product of peroxisomally targeted tNCS is not sequestered in the peroxisome, we showed that it is accessible to the downstream four-enzyme pathway that converts (*S*)-norcoclaurine to (*S*)-reticuline in the cytosol (Fig. 2f). (*S*)-Reticuline represents the last shared intermediate of the large and highly branched family of BIA natural products[9]. To synthesize (*S*)-reticuline, (*S*)-norcoclaurine must undergo two O-methylations, one N-methylation and one hydroxylation, collectively catalyzed by 6-*O*-methyltransferase (6OMT), coclaurine *N*-methyltransferase (CNMT), *N*-methylcoclaurine 3′-hydroxylase (NMCH) and 4′-*O*-methyltransferase (4′OMT), all of which have been functionally expressed and experimentally validated in yeast[17,29]. These four enzymes were cytosolically expressed along with the upstream CYP76AD5 and DODC, with tNCS compartmentalized in either the peroxisome or cytosol. Compared to cytosolic expression (dead_ePTS1), peroxisomal targeting (ePTS1) resulted in a modest growth rate improvement and a 34% increase in final OD (Extended Data Fig. 4). A corresponding production improvement was observed (Fig. 2g), as evidenced by a 2.1-fold increase in titer and a 34% increase in maximum productivity (0.11 versus 0.08 mg liter^{-1} per hour). In general, (*S*)-reticuline titers were higher than (*S*)-norcoclaurine titers. Cell density was also higher for (*S*)-reticuline strains than for (*S*)-norcoclaurine strains (Extended Data Figs. 3 and 4). We attribute these differences to the inclusion of enzymes from the violacein pathway (VioA, VioB and tNCS fused to VioE) in the (*S*)-norcoclaurine strains, whereas the (*S*)-reticuline strains did not contain the violacein enzymes.

Limited capacity for higher tNCS expression levels. While peroxisomal compartmentalization of tNCS was effective at the tested expression levels, we wanted to determine whether the peroxisome is capable of compartmentalizing even higher expression levels to achieve increased titers. Plasmid copy number was increased from that with the CEN6/ARS4 plasmid (2–5 copies) to that with the 2 micron (2μ) plasmid (15–50 copies)[21,30]. At this very high expression level, peroxisomal compartmentalization was still effective but incomplete (Fig. 3). At high 2μ expression levels, colocalization

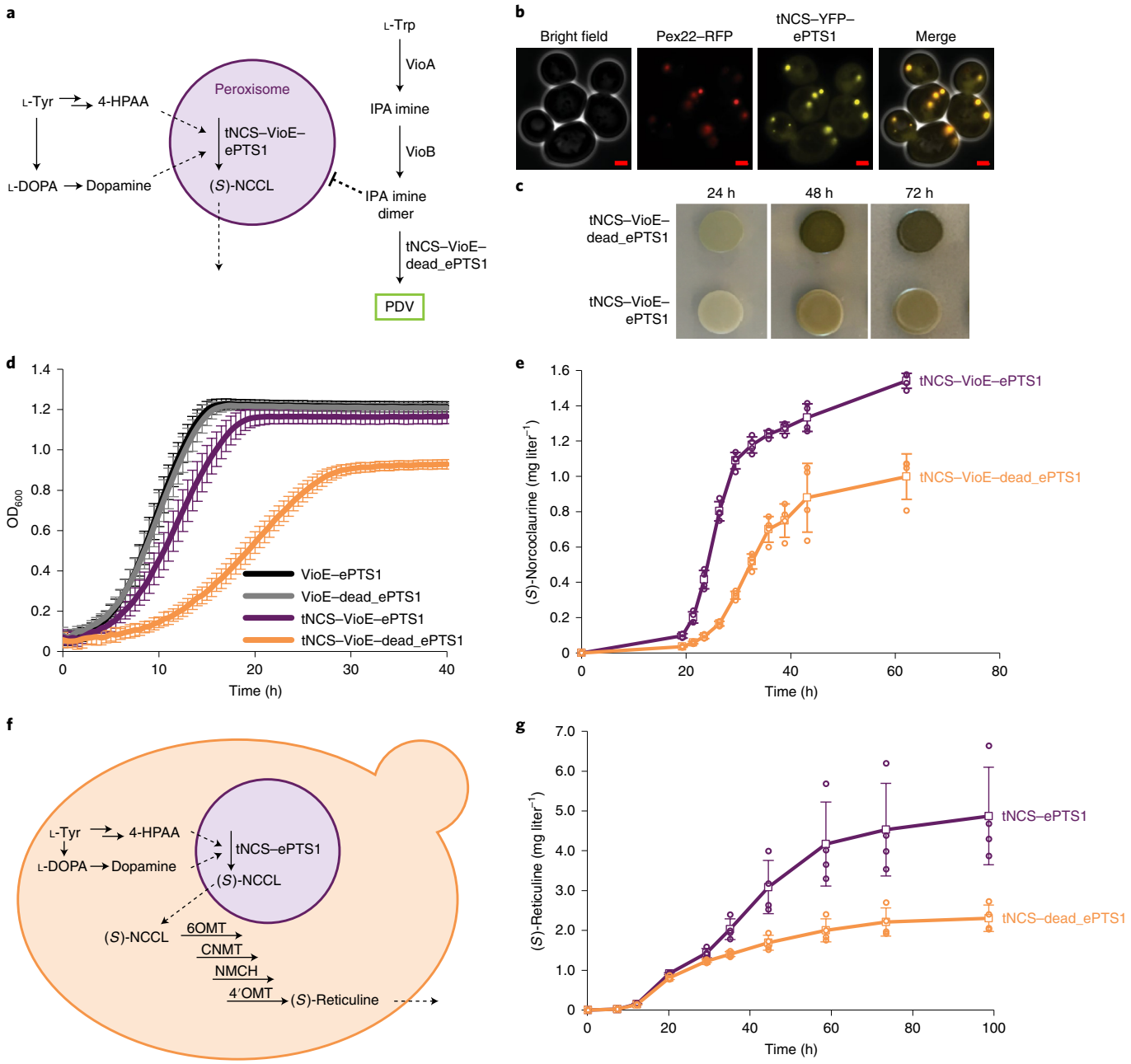

Fig. 2 | Compartmentalizing tNCS in the peroxisome alleviates cytotoxicity and increases product titer. a, The tNCS-VioE fusion protein is targeted to the peroxisome when tagged with ePTS1 but remains in the cytosol when tagged with dead_ePTS1. NCS substrates 4-HPAA and dopamine can access peroxisomal tNCS to produce (*S*)-norcoclaurine ((*S*)-NCCL). The violacein pathway, which is used to assess peroxisomal compartmentalization, includes VioA and VioB expressed in the cytosol. When VioE is also expressed in the cytosol (tNCS-VioE-dead_ePTS1), green PDV pigment is produced. When VioE is targeted to the peroxisome (tNCS-VioE-ePTS1), less PDV is produced because the precursor IPA imine dimer has low permeability across the peroxisomal membrane. **b**, Microscopy showing colocalization of tNCS-YFP-ePTS1 with peroxisomal marker Pex22-RFP. RFP channel brightness was increased to allow visualization in the merged image. Scale bars, 2 µm. The experiment was repeated twice with similar results. **c**, Agar plate spots showing the compartmentalization efficiency of tNCS-VioE-ePTS1 in the peroxisome compared to tNCS-VioE-dead_ePTS1. tNCS-VioE-ePTS1 spots have less green color due to lower production of PDV. **d**, Expression of tNCS in the cytosol (tNCS-VioE-dead_ePTS1, orange line) results in poor growth, whereas compartmentalization in the peroxisome (tNCS-VioE-ePTS1, purple line) alleviates toxicity. Data are shown as the mean ± s.d. of 12 biological replicates. **e**, Peroxisomal compartmentalization of tNCS (tNCS-VioE-ePTS1) results in higher (*S*)-norcoclaurine production than cytosolic expression of tNCS (tNCS-VioE-dead_ePTS1). Data are shown as the mean ± s.d. of four biological replicates. **f**, Pathway for production of (*S*)-reticuline with tNCS-ePTS1 localized in the peroxisome but with free flow of substrates and product across the peroxisomal membrane. All other enzymes are expressed in the cytosol. **g**, Compartmentalizing tNCS-ePTS1 in the peroxisome results in higher (*S*)-reticuline production than with tNCS-dead_ePTS1 expression in the cytosol. Data are shown as the mean ± s.d. of four biological replicates.

of tNCS–YFP–ePTS1 with peroxisomal marker Pex22–RFP was observed (Fig. 3a) but with more residual cytosolic tNCS–YFP–ePTS1, as indicated by increased cytosolic YFP signal compared with that previously observed for CEN6/ARS4 expression (Figs. 2b and 3a). At 2µ expression levels, incomplete compartmentalization and high toxicity were observed in the pigment-producing enzyme

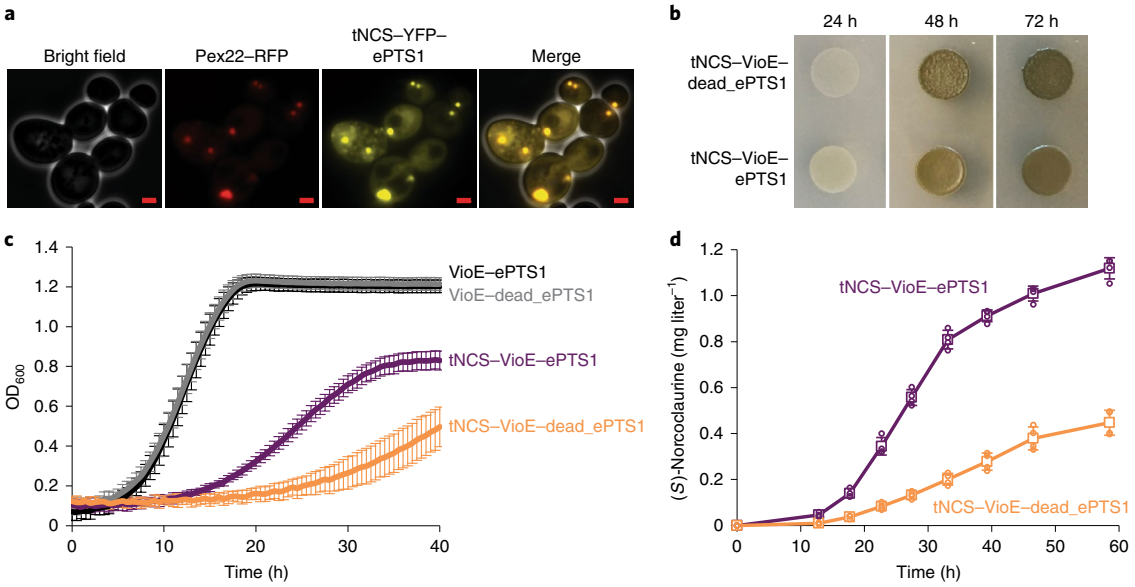

Fig. 3 | Peroxisomal targeting of toxic tNCS at a very high expression level improves growth and (*S*)-norcoclaurine titer, but compartmentalization is incomplete. a, Microscopy showing colocalization of tNCS-YFP-ePTS1 (pTDH3 2μ expression level) with Pex22-RFP at peroxisomes and residual YFP signal in the cytosol (incomplete compartmentalization). RFP channel brightness was increased to allow visualization in the merged image. Scale bars, 2 μm. The experiment was repeated twice with similar results. **b**, Agar plate spots showing the compartmentalization efficiency of tNCS-VioE-ePTS1 in the peroxisome compared with tNCS-VioE-dead_ePTS1. Abnormal spot morphology for cytosolic expression (tNCS-VioE-dead_ePTS1) indicates high toxicity. **c**, Expression of tNCS in the cytosol (tNCS-VioE-dead_ePTS1) results in very poor growth (orange line), whereas peroxisomal targeting (tNCS-VioE-ePTS1) partially alleviates toxicity at the pTDH3 2μ expression level (purple line) when compared with the growth of control strains (black and gray lines). Data are shown as the mean ± s.d. of 12 biological replicates. **d**, Peroxisomal targeting of tNCS (tNCS-VioE-ePTS1) results in higher (*S*)-norcoclaurine production than cytosolic expression of tNCS (tNCS-VioE-dead_ePTS1). Data are shown as the mean ± s.d. of four biological replicates.

sequestration assay and in growth experiments. PDV pigment extraction after 3 d of growth showed a 39% reduction in PDV pigment when tNCS–VioE was targeted to the peroxisome instead of the cytosol (Fig. 3b). Toxicity due to high cytosolic expression of tNCS–VioE was apparent in the agar plate spots and was evidenced by low cell density at 24 h and abnormal spot morphology (wrinkled appearance) at 48 and 72 h. Growth curves showed that cytosolic expression (tNCS–VioE–dead_ePTS1) was highly toxic, and hardly any growth occurred before 20 h, at which point the control strains lacking tNCS (VioE–ePTS1 and VioE–dead_ePTS1) had already reached a saturated cell density (Fig. 3c). Peroxisomal compartmentalization of tNCS (tNCS–VioE–ePTS1) alleviated some of the toxicity, confirming that peroxisome targeting was still effective; however, the final OD and growth rate were lower than those of the control strains, suggesting that the peroxisome is not natively capable of completely compartmentalizing the toxic tNCS at these elevated expression levels.

Production of (*S*)-norcoclaurine was greatly improved upon targeting of tNCS to the peroxisome compared with the cytosol at the 2μ expression level. (*S*)-Norcoclaurine titer was 2.5-fold higher for peroxisomal targeting than with cytosolic expression from a 2μ plasmid (Fig. 3d), and maximum productivity was 3.2-fold higher (0.045 versus 0.014 mg liter^{-1} per hour). However, the titer of peroxisomal expression from a 2μ plasmid was lower than that of peroxisomal CEN6/ARS4 expression (1.1 versus 1.5 mg liter^{-1}). We attribute this lower titer to the poor growth caused by incomplete compartmentalization at the elevated expression level of the 2μ plasmid. Indeed, the final OD and growth rate in flasks were 3.6 and 0.34 h^{-1}, respectively, when tNCS was expressed from a CEN6/ARS4 plasmid, but only 2.7 and 0.14 h^{-1} when it was expressed from a 2μ plasmid (Extended Data Figs. 3 and 5).

Rewiring peroxisome induction for increased capacity. Protein capacity is limited in most organelles, and, although the peroxisome can natively compartmentalize a comparably impressive amount[15], further increased capacity is desired for many applications, including insulation of the toxic tNCS. In *S. cerevisiae*, the natural function of peroxisomes is the β-oxidation of long-chain fatty acids[31]. In glucose-containing media, peroxisomes have an average diameter of 0.2 μm (ref. [32]), but, in media containing the C18 fatty acid oleate, peroxisomes are induced to reach diameters of 0.3–0.5 μm (ref. [33]). Unfortunately, growth in oleate-containing media is poor, but media cannot be supplemented with glucose to improve growth because it represses peroxisome induction[34]. Although we observed peroxisome proliferation in oleate-containing medium as expected (Supplementary Fig. 1), (*S*)-norcoclaurine titer did not improve due to poor growth in oleate-containing medium compared with glucose-containing medium (Supplementary Fig. 2). To circumvent this, we sought to engineer a strain with increased peroxisome capacity while grown on the favored glucose carbon source. We focused on three transcription factors known to control peroxisome proliferation: ADR1, OAF1 and PIP2. All three transcription factors are post-translationally repressed by glucose, and OAF1 is post-translationally induced by oleate[35,36]. We aimed to make ADR1, OAF1 and PIP2 constitutively active in glucose-containing medium and remove the requirement for oleate by engineering or deleting the regulatory domains of these transcription factors.

An engineered version of the ADR1 transcription factor was designed to enable constitutive activation in glucose. ADR1 is inactivated by phosphorylation at Ser230 under high glucose concentrations[35]; activation is achieved by Ser230 dephosphorylation when the glucose concentration is low. Mutation of Ser230 to alanine can mimic the dephosphorylated, active state, leading to transcription of downstream genes even in the presence of glucose[35]. We applied

this S230A mutation to generate ADR1c, a constitutively active version of ADR1.

Engineered versions of OAF1 and PIP2 transcription factors were designed through removal of regulatory domains to enable activation in glucose-containing medium without oleate. OAF1 and PIP2 have similar domain architectures, both containing an N-terminal DNA-binding domain followed by regulatory domains and ending with a C-terminal activation domain[36]. We hypothesized that removal of the regulatory domains would enable constitutive activation in standard media by removing glucose repression and the need for oleate induction. For OAF1, we tethered amino acids 1–100 (containing the DNA-binding domain) via a flexible two-residue glycine–serine linker to amino acids 807–1047 (containing the activation domain). Likewise, for PIP2, we tethered amino acids 1–56 (DNA-binding domain) to amino acids 833–996 (activation domain) via a glycine–serine linker. We called these engineered transcription factors OAF1c and PIP2c, respectively.

These engineered transcription factors activated downstream promoters within the peroxisome proliferation network as expected (Extended Data Fig. 6). The promoter regions of four genes upregulated by ADR1, OAF1/PIP2 or both[37,38] were cloned and used to drive expression of YFP. In a strain that did not contain our engineered transcription factors, these promoters produced very low levels of YFP, consistent with glucose repression. YFP expression from these four promoters increased by 13- to 62-fold in the presence of the engineered transcription factors, whereas YFP expression from constitutive yeast promoters remained stable, demonstrating that ADR1c, OAF1c and PIP2c are able to activate the peroxisome proliferation network in glucose-containing media without oleate induction.

A fluorescence-based assay was devised to test peroxisome compartmentalization capacity upon expression of combinations of the engineered transcription factors. The assay utilizes YFP fused to an N-terminal proteasome-based degradation signal, UbiY[23], and a C-terminal ePTS1 tag (Fig. 4a). In this assay, Pex5p recognizes ePTS1 to shuttle UbiY–YFP–ePTS1 cargo to the peroxisomal membrane for import, where it would be protected from degradation. Residual UbiY–YFP–ePTS1 in the cytosol is degraded by the proteasome. The fluorescent signal should, consequently, only reflect YFP localized in the peroxisome. Therefore, combinations of constitutively active transcription factors resulting in improved cargo capacities will be reflected as increased YFP compared with the signal produced in a strain with no transcription factor overexpression.

The degron–YFP assay functioned as expected; degradation was observed upon cytosolic expression and protection was observed upon peroxisomal targeting. We demonstrated that fusion of the UbiY degron to YFP–ePTS1 resulted in cytosolic degradation by expressing this fusion in a *PEX5*-knockout strain (*pex5*Δ), in which peroxisomal import is prevented (Fig. 4b). Expression of this fusion protein, UbiY–YFP–ePTS1, in a wild-type strain containing Pex5p resulted in 4.2-fold-higher YFP signal (Fig. 4b), indicating protection from degradation due to peroxisomal import.

Engineered transcription factors increased protection of cargo from degradation (Fig. 4b) and resulted in visibly larger peroxisomes with increased fluorescence from importing UbiY degron-fused YFP (Fig. 4c). The engineered transcription factors ADR1c, OAF1c and PIP2c were first expressed in different combinations and strains were assayed for UbiY–YFP–ePTS1 signal after growth for 48 h in a 96-well culture block (Supplementary Fig. 3). The highest YFP signal, indicating improved protection from degradation, was observed upon expression of all three engineered transcription factors. We investigated the dynamics of the system by culturing the triple-transcription factor (TF) strain alongside controls in a small-scale microwell plate (Extended Data Fig. 7). Strains with cytosolic UbiY–YFP–ePTS1 showed an increase in YFP over the first ~15 h during the culture growth phase and, thereafter, showed a drop in YFP as the rate of proteasomal degradation outpaced the rate of YFP synthesis, as expected. Strains with peroxisomal UbiY–YFP–ePTS1 exhibited protection from degradation by showing less YFP degradation after the growth phase, resulting in higher YFP signal at the endpoint relative to their counterpart strains with cytosolic expression. Endpoint values from the time course experiment are depicted in Fig. 4b and show that the TF combination resulted in 2.8-fold-higher UbiY–YFP–ePTS1 fluorescence than without TF expression and 90% of the fluorescence compared to the no-degron strain. We then compared the wild-type background strain to the ADR1c/OAF1c/PIP2c expression strain, both of which expressed UbiY–YFP–ePTS1, by microscopy and found that TF overexpression resulted in larger peroxisomes (Fig. 4c). While there was cell–cell variability with regard to the presence and size of peroxisomes, they were routinely larger and brighter in the TF strain (Extended Data Fig. 8). Thus, increased cargo capacity can be achieved in glucose-containing media through expression of constitutively active versions of transcription factors involved in glucose derepression and oleate induction.

Improved capacity for UbiY–YFP–ePTS1 translated to a 36% improvement in (*S*)-norcoclaurine titer when tNCS was targeted to the peroxisome compared with peroxisome targeting without TF overexpression. We built strains containing the high-copy 2μ plasmid expressing peroxisome-targeted tNCS (pTDH3–tNCS–ePTS1) in either a wild-type strain background or a strain overexpressing the best set of transcription factors (ADR1c, OAF1c and PIP2c). Transcription factor overexpression resulted in a 36% increase in (*S*)-norcoclaurine titer compared with the wild-type strain without TF overexpression (Fig. 4d). Although we did not observe the expected increase in growth upon expression of constitutively active ADR1c, OAF1c and PIP2c (Extended Data Fig. 9), we noted that TF overexpression caused a decrease in growth even in the absence of toxic tNCS (Extended Data Fig. 10). Thus, one or more of the >100 genes regulated by these transcription factors presents a burden or directly inhibits growth[37,38]. When normalized by OD, expression of the engineered TFs resulted in a 47% improvement in (*S*)-norcoclaurine production (Extended Data Fig. 9). Ultimately, the benefit of TF overexpression on peroxisome size and capacity outweighed the growth defect, resulting in higher (*S*)-norcoclaurine titer.

Discussion

Toxicity of heterologous proteins[39–41] and metabolites[42–44] is a notable problem in metabolic engineering. Toxicity manifests as substantial obstructions to large-scale fermentation in terms of slower growth and ultimately lower titer and productivity. We faced the challenge of needing to highly express tNCS enzyme to improve the titer of BIAs while discovering that high expression of tNCS also caused cytotoxicity in *S. cerevisiae*. This challenge required a specific solution in which tNCS would be efficiently targeted and sequestered but retain access to its small molecule substrates and allow the (*S*)-norcoclaurine product to exit to the cytosol where the downstream enzymes are localized. One approach could involve the use of a compartment that is not readily permeable to small molecules (for example, vacuole[45]) and compartmentalization of the entire metabolic pathway. However, in addition to the requirement for high protein capacity that has not been demonstrated for most organelles, this approach would necessitate the incorporation of one or several transporters recognizing the enzyme's substrate(s) and, potentially, product at the organelle membrane.

Peroxisomal compartmentalization has the potential to be a generalizable strategy for the expression of toxic proteins. The mechanism of tNCS toxicity is unknown, and, in general, the mechanisms causing toxicity in engineered systems can be difficult to elucidate. A common strategy for minimizing, or even overcoming, this undesired effect on the production host is to conduct adaptive laboratory evolution (ALE)[46]. ALE works best when the desired flux can

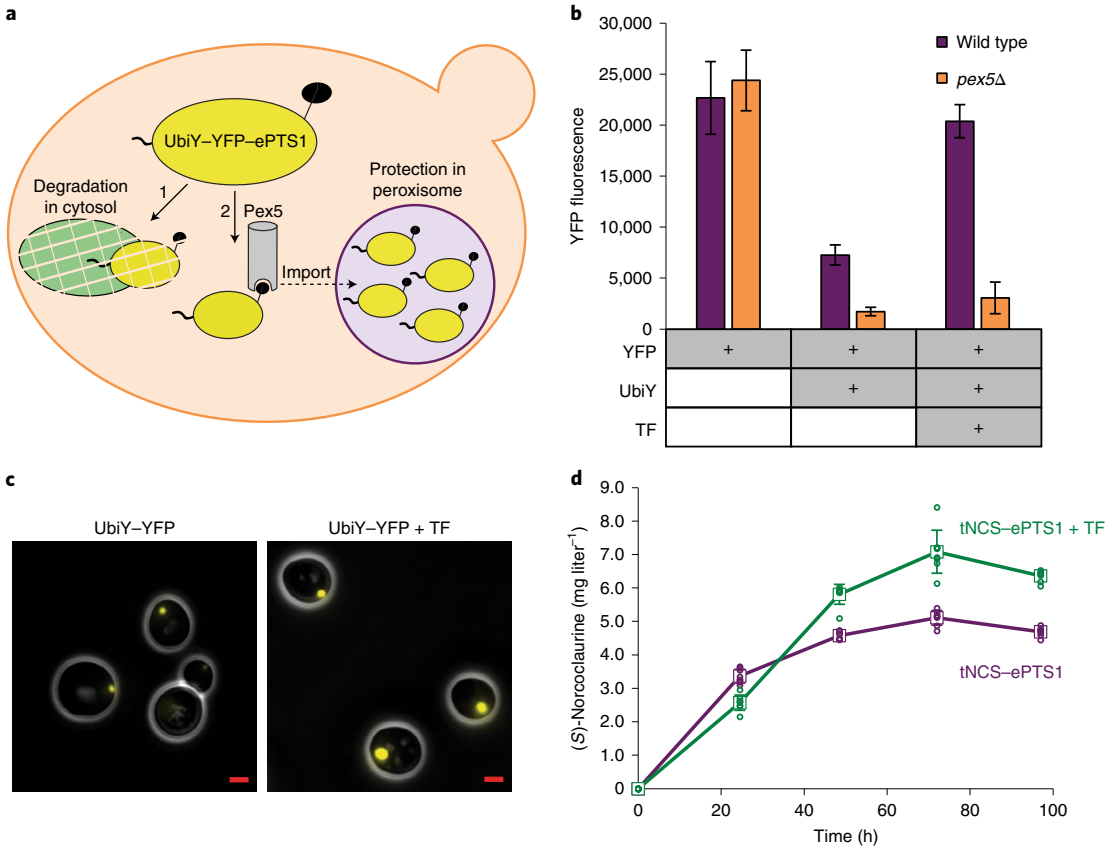

Fig. 4 | Genetic induction of peroxisome proliferation can address incomplete compartmentalization at very high expression levels of tNCS. a, Degron-YFP assay for measuring peroxisomal compartmentalization. Residual UbiY-YFP-ePTS1 that is not imported to the peroxisome by Pex5p (path 2) is degraded in the cytosol by the proteasome (path 1). Changes in YFP signal are therefore indicative of changes in peroxisome import capacity. **b**, The degron-YFP assay was used to assess transcription factor overexpression. Strains with UbiY-YFP-ePTS1 in the cytosol (*pex5*Δ) have lower fluorescence than corresponding strains with peroxisomally targeted YFP (wild type) due to UbiY-YFP degradation by the proteasome. TF represents expression of engineered transcription factors ADR1c, OAF1c and PIP2c. Data are shown as the mean ± s.d. of 12 biological replicates. **c**, Microscopy of UbiY-YFP-ePTS1 cells shows larger peroxisomes when ADR1c, OAF1c and PIP2c are expressed (TF). YFP channel brightness was increased identically across both images to allow better visualization of peroxisomes from the UbiY-YFP strain. Scale bars, 10 µm. The experiment was repeated four times with similar results. Full images showing population variability are available in Extended Data Fig. 8. **d**, (*S*)-Norcoclaurine production is improved upon expression of engineered transcription factors. Data are shown as the mean ± s.d. of eight biological replicates.

be selected such that derived mutations for improved growth are not exclusive with pathway flux, and ALE can fail if growth is improved at the expense of product titer[47]. ALE often requires months of cell passaging to enable mutations to be acquired, especially when the acquisition of multiple mutations is required[46]. If the mechanism of toxicity is well understood, a more rational solution may be developed, such as a mutation to the protein to block undesired interactions or a genetic modification (gene deletion or mutation) that reduces toxicity. Peroxisome compartmentalization is a considerably more rapid strategy, requiring only the addition of the C-terminal ePTS1 tag, and does not require understanding of the mechanism of toxicity other than determining that it is due to the protein and not a small metabolite. This strategy should be generalizable to all soluble proteins directly exerting toxicity (that is via interactions with protein(s), lipid(s), carbohydrate(s) and so on that are accessible in the cytosol).

The *S. cerevisiae* peroxisome has evolved for the compartmentalization of enzymes induced for the β-oxidation of long-chain fatty acids[31]. Examples in nature indicate that the peroxisome is an inherently flexible organelle, serving as the location for unique biochemical reactions such as penicillin biosynthesis[48] and generation of light in fireflies[12] and, therefore, likely has the potential to be engineered as a synthetic compartment for desired applications. Moreover, peroxisome size, number and morphology can be substantially altered in different organisms using a variety of substrates such as oleate[33], methanol[49] and butyrate[50], indicating that genetic circuits for peroxisome proliferation are prevalent across a broad range of eukaryotes. We pursued genetic reprogramming of peroxisome proliferation via constitutive expression of engineered transcription factors and demonstrated increased cargo capacity without the requirement for oleate. Although this is an important step toward genetic control over peroxisome cargo capacity, expression of these constitutively active transcription factors resulted in a decrease in growth even in the absence of toxic tNCS. Given that >100 downstream genes are regulated by these transcription factors, it is unsurprising that one or more may have an impact on cell state/growth[37,38]. Future work will seek to identify the most important downstream targets of ADR1, OAF1 and PIP2 such that only the critical genes will be manipulated to control cargo capacity without impeding growth.

This work establishes a robust strategy for circumventing the growth defect resulting from the expression of a cytotoxic metabolic enzyme while enabling increased flux. Protection of heterologous cargo from the effects of the host cell, such as proteasome-based degradation, was also demonstrated. Peroxisome compartmentalization offers the engineer bidirectional benefits: protection of the host cell from the heterologous protein as well as protection of the

heterologous protein from the host cell. This work highlights the peroxisome as a versatile, engineerable organelle that can be utilized to address challenges in metabolic engineering.

Online content

Any methods, additional references, Nature Research reporting summaries, source data, extended data, supplementary information, acknowledgements, peer review information; details of author contributions and competing interests; and statements of data and code availability are available at https://doi.org/10.1038/s41589-020-00668-4.

Received: 27 February 2020; Accepted: 2 September 2020;
Published online: 12 October 2020

References

1. Li, F., Vijayasankaran, N., Shen, A., Kiss, R. & Amanullah, A. Cell culture processes for monoclonal antibody production. *MAbs* **2**, 466–479 (2010).
2. Meadows, A. L. et al. Rewriting yeast central carbon metabolism for industrial isoprenoid production. *Nature* **537**, 694–697 (2016).
3. Sauer, M. Industrial production of acetone and butanol by fermentation—100 years later. *FEMS Microbiol. Lett.* **363**, 1–4 (2016).
4. Eibl, R. et al. Plant cell culture technology in the cosmetics and food industries: current state and future trends. *Appl. Microbiol. Biotechnol.* **102**, 8661–8675 (2018).
5. Yeates, T. O., Thompson, M. C. & Bobik, T. A. The protein shells of bacterial microcompartment organelles. *Curr. Opin. Struct. Biol.* **21**, 223–231 (2011).
6. Hammer, S. K. & Avalos, J. L. Harnessing yeast organelles for metabolic engineering. *Nat. Chem. Biol.* **13**, 823–832 (2017).
7. Hecht, K. A., O'Donnell, A. F. & Brodsky, J. L. The proteolytic landscape of the yeast vacuole. *Cell Logist.* **4**, e28023 (2014).
8. Haanstra, J. R. et al. Compartmentation prevents a lethal turbo-explosion of glycolysis in trypanosomes. *Proc. Natl Acad. Sci. USA* **105**, 17718–17723 (2008).
9. Hagel, J. M. & Facchini, P. J. Benzylisoquinoline alkaloid metabolism: a century of discovery and a brave new world. *Plant Cell Physiol.* **54**, 647–672 (2013).
10. Lichman, B. R. et al. Dopamine-first mechanism enables the rational engineering of the norcoclaurine synthase aldehyde activity profile. *FEBS J.* **282**, 1137–1151 (2015).
11. DeLoache, W. C., Russ, Z. N. & Dueber, J. E. Towards repurposing the yeast peroxisome for compartmentalizing heterologous metabolic pathways. *Nat. Commun.* **7**, 11152 (2016).
12. Subramani, S. Targeting of proteins into the peroxisomal matrix. *J. Membr. Biol.* **125**, 99–106 (1992).
13. Kohlwein, S. D., Veenhuis, M. & van der Klei, I. J. Lipid droplets and peroxisomes: key players in cellular lipid homeostasis or a matter of fat-store'em up or burn'em down. *Genetics* **193**, 1–50 (2013).
14. Distel, B. & Kragt, A. *Purification of yeast peroxisomes*. in *Methods in Molecular Biology*, Vol. 313 (ed. Xiao, W.) https://doi.org/10.1385/1-59259-958-3:021 (Humana Press, 2006).
15. Ehrenworth, A. M., Haines, M. A., Wong, A. & Peralta-Yahya, P. Quantifying the efficiency of *Saccharomyces cerevisiae* translocation tags. *Biotechnol. Bioeng.* **114**, 2628–2636 (2017).
16. Antonenkov, V. D., Sormunen, R. T. & Hiltunen, J. K. The rat liver peroxisomal membrane forms a permeability barrier for cofactors but not for small metabolites in vitro. *J. Cell. Sci.* **117**, 5633–5642 (2004).
17. DeLoache, W. C. et al. An enzyme-coupled biosensor enables (*S*)-reticuline production in yeast from glucose. *Nat. Chem. Biol.* **11**, 465–471 (2015).
18. Samanani, N., Liscombe, D. K. & Facchini, P. J. Molecular cloning and characterization of norcoclaurine synthase, an catalyzing the first committed step in benzylisoquinoline alkaloid biosynthesis. *Plant J.* **40**, 302–314 (2004).
19. Nishihachijo, M. et al. Asymmetric synthesis of tetrahydroisoquinolines by enzymatic Pictet–Spengler reaction. *Biosci. Biotechnol. Biochem.* **78**, 701–707 (2014).
20. Li, Y. et al. Complete biosynthesis of noscapine and halogenated alkaloids in yeast. *Proc. Natl Acad. Sci. USA* **115**, E3922–E3931 (2018).
21. Karim, A. S., Curran, K. A. & Alper, H. S. Characterization of plasmid burden and copy number in *Saccharomyces cerevisiae* for optimization of metabolic engineering applications. *FEMS Yeast Res.* **13**, 107–116 (2013).
22. Lee, M. E., Aswani, A., Han, A. S., Tomlin, C. J. & Dueber, J. E. Expression-level optimization of a multi-enzyme pathway in the absence of a high-throughput assay. *Nucleic Acids Res.* **41**, 10668–10678 (2013).
23. Lee, M. E., DeLoache, W. C., Cervantes, B. & Dueber, J. E. A highly characterized yeast toolkit for modular, multipart assembly. *ACS Synth. Biol.* **4**, 975–986 (2015).
24. Ruff, B. M., Bräse, S. & O'Connor, S. E. Biocatalytic production of tetrahydroisoquinolines. *Tetrahedron Lett.* **53**, 1071–1074 (2012).
25. Pesnot, T., Gershater, M. C., Ward, J. M. & Hailes, H. C. The catalytic potential of *Coptis japonica* NCS2 revealed—development and utilisation of a fluorescamine-based assay. *Adv. Synth. Catal.* **354**, 2997–3008 (2012).
26. Ramirez-Gaona, M. et al. YMDB 2.0: a significantly expanded version of the yeast metabolome database. *Nucleic Acids Res.* **45**, D440–D445 (2017).
27. Walton, P. A., Hill, P. E. & Subramani, S. Import of stably folded proteins into peroxisomes. *Mol. Biol. Cell* **6**, 675–683 (1995).
28. Halbach, A., Rucktächel, R., Rottensteiner, H. & Erdmann, R. The N-domain of Pex22p can functionally replace the Pex3p N-domain in targeting and peroxisome formation. *J. Biol. Chem.* **284**, 3906–3916 (2009).
29. Galanie, S., Thodey, K., Trenchard, I. J., Interrante, M. F. & Smolke, C. D. Complete biosynthesis of opioids in yeast. *Science* **349**, 1095–1100 (2015).
30. Chan, K. M., Liu, Y. T., Ma, C. H., Jayaram, M. & Sau, S. The 2 micron plasmid of *Saccharomyces cerevisiae*: a miniaturized selfish genome with optimized functional competence. *Plasmid* **70**, 2–17 (2013).
31. Kunau, W. H., Dommes, V. & Schulz, H. β-Oxidation of fatty acids in mitochondria, peroxisomes, and bacteria: a century of continued progress. *Prog. Lipid Res.* **34**, 267–342 (1995).
32. Yofe, I. et al. Pex35 is a regulator of peroxisome abundance. *J. Cell. Sci.* **130**, 791–804 (2017).
33. Vizeacoumar, F., Torres-Guzman, J., Bouard, D., Aitchison, J. & Rachubinski, R. Pex30p, Pex31p, and Pex32p form a family of peroxisomal integral membrane proteins regulating peroxisome size and number in *Saccharomyces cerevisiae*. *Mol. Biol. Cell* **15**, 665–677 (2004).
34. Grillitsch, K. et al. Lipid particles/droplets of the yeast *Saccharomyces cerevisiae* revisited: lipidome meets proteome. *Biochim. Biophys. Acta Mol. Cell Biol. Lipids* **1811**, 1165–1176 (2011).
35. Ratnakumar, S. & Young, E. T. Snf1 dependence of peroxisomal gene expression is mediated by Adr1. *J. Biol. Chem.* **285**, 10703–10714 (2010).
36. Baumgartner, U., Hamilton, B., Piskacek, M., Ruis, H. & Rottensteiner, H. Functional analysis of the Zn_2Cys_6 transcription factors Oaf1p and Pip2p. *J. Biol. Chem.* **274**, 22208–22216 (1999).
37. Young, E. T., Dombek, K. M., Tachibana, C. & Ideker, T. Multiple pathways are co-regulated by the protein kinase Snf1 and the transcription factors Adr1 and Cat8. *J. Biol. Chem.* **278**, 26146–26158 (2003).
38. Trzcinska-Danielewicz, J., Ishikawa, T., Miciałkiewicz, A. & Fronk, J. Yeast transcription factor Oaf1 forms homodimer and induces some oleate-responsive genes in absence of Pip2. *Biochem. Biophys. Res. Commun.* **374**, 763–766 (2008).
39. Miroux, B. & Walker, J. E. Over-production of proteins in *Escherichia coli*: mutant hosts that allow synthesis of some membrane proteins and globular proteins are high levels. *J. Membr. Biol.* **260**, 289–298 (1996).
40. Outeiro, T. F. & Lindquist, S. Yeast cells provide insight into α-synuclein biology and pathobiology. *Science* **302**, 1772–1775 (2003).
41. Ju, S. *et al*. A yeast model of FUS/TLS-dependent cytotoxicity. *PLoS Biol.* **9**, e1001052 (2011).
42. Martin, V. J., Pitera, D. J., Withers, S. T., Newman, J. D. & Keasling, J. D. Engineering a mevalonate pathway in *Escherichia coli* for production of terpenoids. *Nat. Biotechnol.* **21**, 796–802 (2003).
43. Ajikumar, P. K. et al. Isoprenoid pathway optimization for Taxol precursor overproduction in *Escherichia coli*. *Science* **330**, 70–74 (2010).
44. Brochado, A. R. et al. Improved vanillin production in baker's yeast through in silico design. *Microb. Cell Fact.* **9**, 1–15 (2010).
45. Li, S. C. & Kane, P. M. The yeast lysosome-like vacuole: endpoint and crossroads. *Biochim. Biophys. Acta Mol. Cell Res.* **1793**, 650–663 (2009).
46. Dragosits, M. & Mattanovich, D. Adaptive laboratory evolution—principles and applications for biotechnology. *Microb. Cell Fact.* **12**, 1–17 (2013).
47. Bentley, G. J. et al. Engineering glucose metabolism for enhanced muconic acid production in *Pseudomonas putida* KT2440. *Metab. Eng.* **59**, 64–75 (2020).
48. Meijer, W. H. et al. Peroxisomes are required for efficient penicillin biosynthesis in *Penicillium chrysogenum*. *Appl. Environ. Microbiol.* **76**, 5702–5709 (2010).
49. Veenhuis, M., Keizer, I. & Harder, W. Characterization of peroxisomes in glucose-grown *Hansenula polymorpha* and their development after the transfer of cells into methanol-containing media. *Arch. Microbiol.* **120**, 167–175 (1979).
50. Weng, H., Endo, K., Li, J., Kito, N. & Iwai, N. Induction of peroxisomes by butyrate-producing probiotics. *PLoS ONE* **10**, 1–11 (2015).

Methods

Strains and growth media. The base *S. cerevisiae* strain for all experiments was BY4741 (*MATa his3Δ1 leu2Δ0 met15Δ0 ura3Δ0*). Base strain BY4741 and BY4741 *pex5Δ* were ordered from Open Biosystems (GE Dharmacon). Wild-type yeast cultures were grown in YPD medium (10 g liter^{-1} Bacto yeast extract, 20 g liter^{-1} Bacto peptone, 20 g liter^{-1} glucose). Selection of auxotrophic markers (*URA3*, *LEU2*, *HIS3*) was performed in synthetic complete (SC) medium (6.7 g liter^{-1} Difco Yeast Nitrogen Base without amino acids (Spectrum Chemical); 2 g liter^{-1} Drop-out Mix Synthetic minus appropriate amino acids, without Yeast Nitrogen Base (US Biological); 20 g liter^{-1} glucose). All strains used in this work are listed in Supplementary Table 1.

Oleate induction medium was prepared as 6.7 g liter^{-1} Difco Yeast Nitrogen Base without amino acids (Spectrum Chemical) and 2 g liter^{-1} Drop-out Mix Synthetic minus appropriate amino acids, without Yeast Nitrogen Base (US Biological), and with the following variations (final concentrations described): (1) 2% glucose; (2) 10% glycerol, 0.1% oleic acid and 0.4% Tween-80; (3) 0.5% glucose, 10% glycerol, 0.1% oleic acid and 0.4% Tween-80.

GoldenGate assembly reactions were transformed into chemically competent *Escherichia coli* prepared from strain TG1 (Lucigen). Transformed cells were selected on LB containing the antibiotics chloramphenicol, ampicillin or kanamycin.

Yeast strain construction. Yeast expression vectors were built using GoldenGate assembly as described in the Yeast Toolkit (YTK) system[23]. Integration into the yeast genome via homologous recombination at the *URA3* or *LEU2* locus was achieved by transformation of linearized plasmids (NotI digestion, NEB), whereas replicating CEN6/ARS4 or 2μ plasmids were transformed directly into yeast without predigestion with NotI. All transformations were performed using a standard lithium acetate method, and cells were plated onto selective auxotrophic SC agar plates with 2% glucose. All strains are described in Supplementary Table 1. Individual colonies (biological replicates) were picked directly from this transformation plate and grown independently for further analysis.

Chromosomal integrations of constructs encoding Pex22–RFP, VioA and VioB were performed by cotransforming a CEN6/ARS4 CRISPR plasmid (containing Cas9, a guide RNA for targeting the appropriate locus and a *HIS3* auxotrophic marker) with linearized repair DNA designed to integrate the gene(s) of interest. Cells were plated on histidine-dropout medium, restreaked on histidine-dropout medium and then grown in non-selective medium to remove the CRISPR plasmid. Chromosomal integration was confirmed by PCR, and removal of CRISPR plasmid was confirmed by replica plating from non-selective medium onto histidine-dropout medium (a colony will not grow on histidine-dropout medium if the CRISPR plasmid has been removed).

Growth curves in microwell plates. Individual colonies were grown to saturation in SC medium with 2% glucose and auxotrophic selection at 30 °C with shaking. Saturated cultures were then diluted 50-fold in fresh selective medium and grown for 6–7 h before a second dilution (10-fold) in 96-well Costar microplates (black, clear bottom), which were sealed with breathe-easy film (Sigma). OD_{600} was measured at 30-min intervals using a microplate reader (Tecan Spark with SparkControl v2.3 or SparkControl v1.2.20 software) and continuous orbital shaking at 30 °C in a humidity cassette. Variation between biological replicates was calculated as the s.d. of the mean OD_{600} at each time point in Microsoft Excel and represented as error bars in figures.

Fluorescence microscopy. For confirmation of protein localization, strains were grown to saturation in SC medium with 2% glucose and auxotrophic selection, diluted 50-fold into fresh selective medium and grown for a further 6–8 h. Cultures were resuspended in 1× PBS before spotting onto plain glass slides for imaging on a Zeiss Axio Observer D1 microscope with an X-Cite Series 120 fluorescent lamp, a Hamamatsu Orca-Flash 4.0 digital camera and ZEN 2.6 (blue edition) software. Images were analyzed using ZEN 3.0 (blue edition) software. The fluorescent protein variants used in this study were YFP Venus and RFP mRuby2.

Spot assays for PDV production and PDV quantification. Agar plate spots for visualization of PDV production were generated by plating 5 μl of saturated culture on SC agar plates with 2% glucose and appropriate auxotrophic selection. Plates were grown at 30 °C and imaged at 24, 48 and 72 h. For PDV quantification, strains were grown to saturation at 30 °C with shaking in SC medium with 2% glucose and auxotrophic selection. Saturated cultures were then diluted 50-fold into fresh selective medium and grown for a further 72 h before PDV extraction was performed as previously described[11]. Relative PDV quantification was determined using bulk fluorescence measurements with 100-μl extracts on a microplate reader (Tecan Infinite M1000 Pro with i-control 1.10 software) with excitation at 535/5 nm and emission at 585/5 nm. PDV production can be estimated using fluorescence measurements at these wavelengths due to a linear correlation to extracts quantified by HPLC[11]. A minimum of six biological replicates of each strain was used for PDV quantification.

BIA production in 96-well culture blocks. (*S*)-Norcoclaurine production experiments for Figs. 1b and 4d, Extended Data Fig. 1, Supplementary Fig. 2 and Extended Data Fig. 9 were performed in 96-well culture blocks. Individual colonies were grown to saturation at 30 °C in selective medium before 50-fold dilution into fresh selective medium. For Fig. 1b and Extended Data Fig. 1, cultures were grown for 72 h after the 50-fold dilution. For Supplementary Fig. 2, cultures were grown for 160 h after the 50-fold dilution. For Fig. 4d and Extended Data Fig. 9, the inoculation culture was diluted 50-fold into a separate block for each time point. At each time point or at final harvest, samples were taken for measurement of OD_{600} on a microplate reader (Tecan Infinite M1000 Pro with i-control 1.10 software). The remaining culture was centrifuged at 4,000*g* and the supernatant was filtered with an Acroprep Advance 0.2-μl filter plate (Pall Corporation). Eight-point standard curves using an (*S*)-norcoclaurine chemical standard (Bepharm) were generated as twofold serial dilutions prepared in culture medium and were used to convert LC–MS peak area to concentration. Samples and standards were diluted in water before LC–MS analysis to achieve concentrations within the linear range of detection of the instrument. Data shown are the mean (*S*)-norcoclaurine titer for 3–8 biological replicates of each strain (as indicated in each figure legend) and error bars represent s.d. of the mean calculated in Microsoft Excel.

BIA production in shake flasks. Shake flask fermentation experiments were performed for (*S*)-norcoclaurine production with tNCS expressed at the CEN6/ARS4 level (Fig. 2e and Extended Data Fig. 3), (*S*)-reticuline production with tNCS at the CEN6/ARS4 level (Fig. 2g and Extended Data Fig. 4) and (*S*)-norcoclaurine with tNCS at the 2μ level (Fig. 3d and Extended Data Fig. 5). Individual colonies were grown to saturation at 30 °C in selective medium. For Fig. 2e and Extended Data Fig. 3, saturated cultures were diluted 500-fold into 50 ml selective medium in 250-ml baffled shake flasks. For all other experiments, saturated cultures were diluted to a starting OD of 0.05 in 50 ml selective medium in 250-ml baffled shake flasks. Shake flask cultures were grown at 30 °C with shaking at 220 r.p.m. in an Innova 44 incubator (Eppendorf). At each time point, samples were taken for measurement of OD_{600} (Thermo Scientific Genesys 30 spectrophotometer) and BIA production. BIA samples were processed as described above for LC–MS and compared with an (*S*)-norcoclaurine or (*S*)-reticuline (ChemCruz) standard curve for quantification.

Fluorescence measurements. Individual colonies were grown to saturation in SC medium with 2% glucose and auxotrophic selection at 30 °C with shaking. Saturated cultures were then diluted 50-fold in fresh medium to a final volume of 500 μl in Corning 96-well culture blocks (cat. no. 07-200-700) and incubated at 30 °C with shaking at 750 r.p.m. To sample OD_{600} and YFP fluorescence, 100 μl was aliquotted into 96-well Costar microplates (black, clear bottom) and measured on a Tecan Infinite M1000 Pro plate reader with i-control 1.10 software. YFP fluorescence was measured using an excitation wavelength of 515 nm and an emission wavelength of 528 nm (5-nm bandwidth for excitation and emission). Variation between biological replicates was calculated as the s.d. of the mean in Microsoft Excel and represented as error bars in figures.

Measurement of the dynamics of degron–YFP was performed as above for growth curves in microwell plates but included the measurement of YFP in addition to OD_{600} at every time point. YFP fluorescence was measured using an excitation wavelength of 513 nm (5-nm bandwidth) and an emission wavelength of 531 nm (7.5-nm bandwidth).

Liquid chromatography–mass spectrometry analysis. LC–MS was performed using a 1260 Infinity LC System connected to a 6120 Quadrupole Mass Spectrometer with Chem Station B.03.04-SP1 software (Agilent Technologies). All samples and standards were diluted in water before injection to achieve linear calibration curves for (*S*)-norcoclaurine and (*S*)-reticuline, with all samples falling within the bounds of the calibration curve. Ten microliters of each diluted sample was injected and sample separation was achieved using a Zorbax Eclipse Plus C18 guard column (4.6 cm × 12.5 cm, 5-μm packing, Agilent Technologies) connected to a Zorbax Eclipse Plus C18 column (4.6 mm × 100 mm, 3.5-μm packing, Agilent Technologies) at ambient temperature using a 0.5 ml min^{-1} flow rate. Samples were eluted with a linear gradient from 100% water/0% acetonitrile plus 0.1% formic acid to 65% water/35% acetonitrile plus 0.1% formic acid over the course of 15 min. MS was conducted in atmospheric pressure ionization-positive electrospray mode at a fragmentor voltage of 100 V with ion detection set to targeted detection of (*S*)-norcoclaurine (272.1 *m*/*z*) and/or (*S*)-reticuline (330.2 *m*/*z*).

Reporting Summary. Further information on research design is available in the Nature Research Reporting Summary linked to this article.

Data availability

The datasets generated and analyzed during the current study are available from the corresponding author on reasonable request. Plasmids are available through Addgene under deposit number 78460.

Acknowledgements

We thank members of the Dueber laboratory for valuable assistance and feedback throughout this project, particularly Z. Russ for training and K. Siu for useful discussions; S. Dupuis for construction of the Pex22–RFP strain; and members of the Wenjun Zhang

laboratory for assistance with LC–MS, particularly W. Skyrud and A. Del Rio Flores. This work is supported by NSF grant MCB 1818307 and by the Center for Cellular Construction, an NSF Science and Technology Center, under grant agreement DBI-1548297.

Author contributions

P.S.G., J.A.S., J.J.B. and J.E.D. designed the research. P.S.G. performed BIA production experiments, growth curves, microscopy, fluorescence measurements, metabolite feeding experiments and cloning. J.A.S. performed growth curves, microscopy, PDV experiments and cloning. J.J.B. performed microscopy, preliminary TF fluorescence measurements and cloning. B.C. assisted with cloning and preliminary experiments. P.S.G., J.A.S. and J.J.B. analyzed the results. J.E.D. supervised the research. P.S.G., J.A.S., J.J.B. and J.E.D. wrote the manuscript.

Competing interests

J.E.D. declares competing financial interests in the form of a pending patent application, US application no. 62/094,877.

Additional information

Extended data is available for this paper at https://doi.org/10.1038/s41589-020-00668-4.

Supplementary information is available for this paper at https://doi.org/10.1038/s41589-020-00668-4.

Correspondence and requests for materials should be addressed to J.E.D.

Reprints and permissions information is available at www.nature.com/reprints.

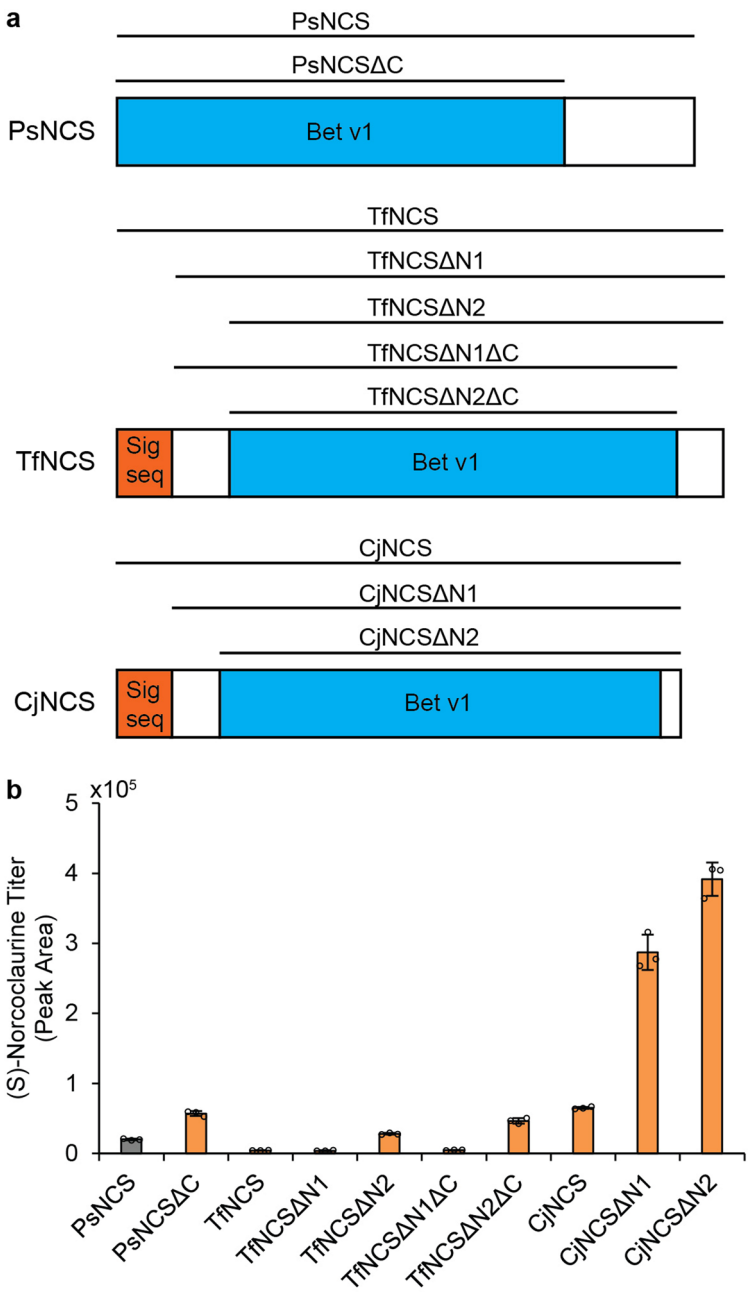

Extended Data Fig. 1 | NCS homologues and truncated variants. a, Truncation strategy for NCS homologues from *Papaver somniferum* (Ps), *Thalictrum flavum* (Tf), and *Coptis japonica* (Cj). Signal sequence (Sig seq) and Bet v1 domains were identified using the SMART domain analysis tool. **b**, (*S*)-Norcoclaurine production by each NCS variant at 72 hours. Gray bar shows our original NCS from *Papaver somniferum*[17]. Error bars represent mean ± s.d. of three biological replicates.

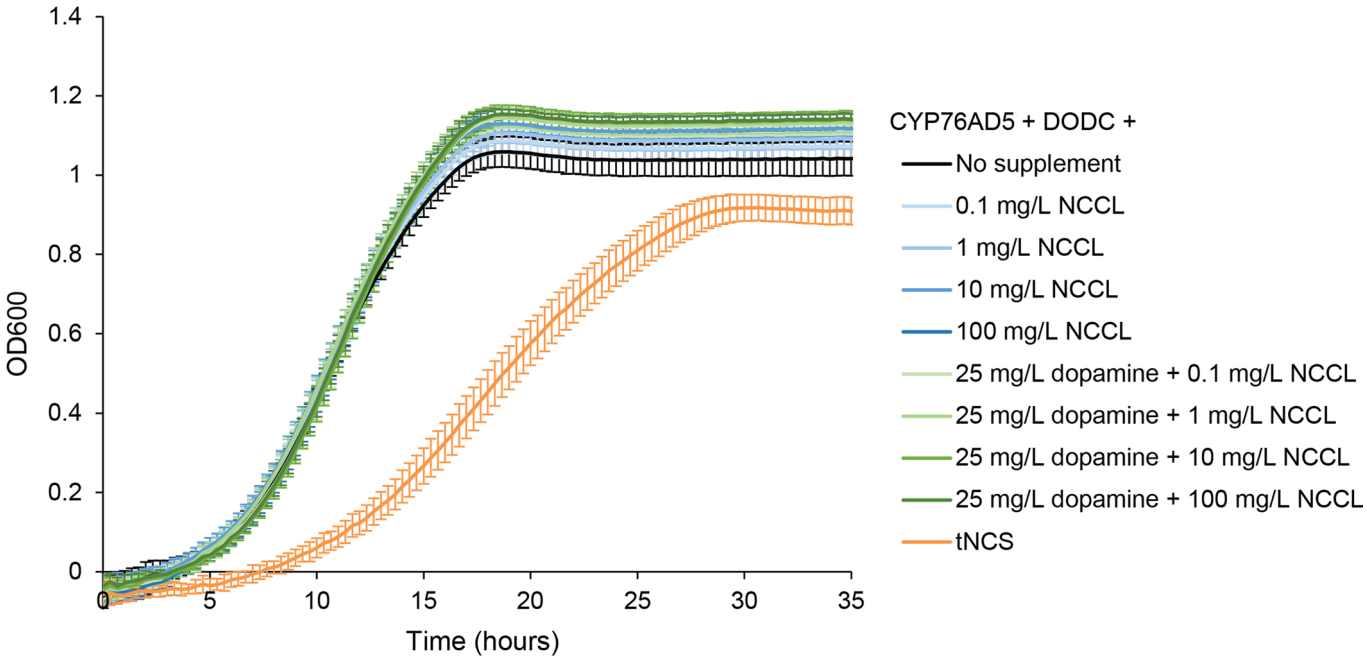

Extended Data Fig. 2 | Dopamine and norcoclaurine are not toxic to *S. cerevisiae* at relevant concentrations. All strains produce dopamine due to expression of CYP76AD5 and DODC. Norcoclaurine (NCCL) was supplemented in the growth media from 0.1 to 100 mg/L. Additional dopamine was supplemented at 25 mg/L to match the production level previously reported[17]. Only expression of tNCS causes slower growth. Error bars represent mean ± s.d. of seven (No supplement, black line) or eight (all others) biological replicates.

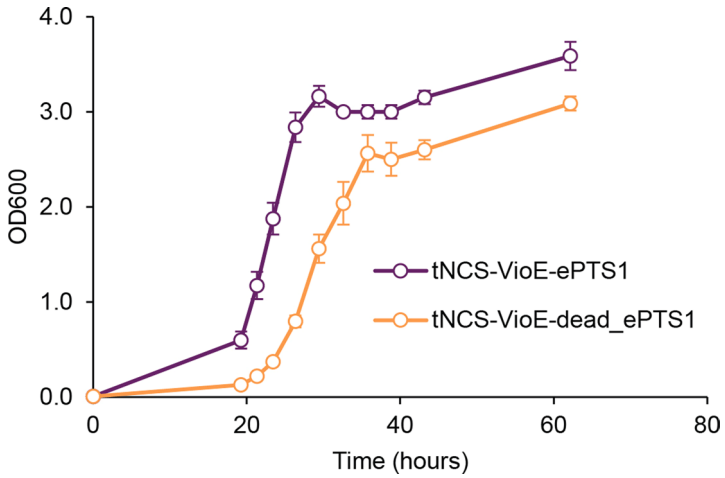

Extended Data Fig. 3 | OD data from (*S*)-norcoclaurine shake flask fermentation experiment. tNCS-VioE-ePTS1 and -dead_ePTS1 constructs were expressed using the strong pTDH3 promoter on a CEN6/ARS4 plasmid. Error bars represent mean ± s.d. of four biological replicates.

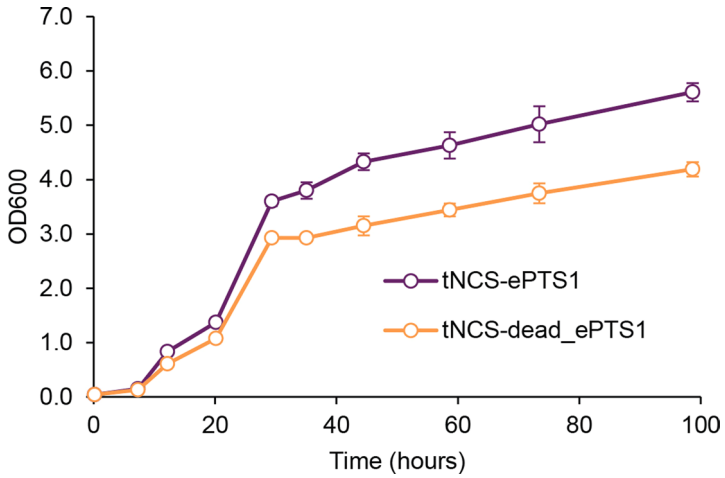

Extended Data Fig. 4 | OD data from (*S*)-reticuline shake flask fermentation experiment. tNCS-ePTS1 and -dead_ePTS1 constructs, along with 6OMT, CNMT, NMCH, and 4'OMT, were expressed on a CEN6/ARS4 plasmid. Error bars represent mean ± s.d. of four biological replicates.

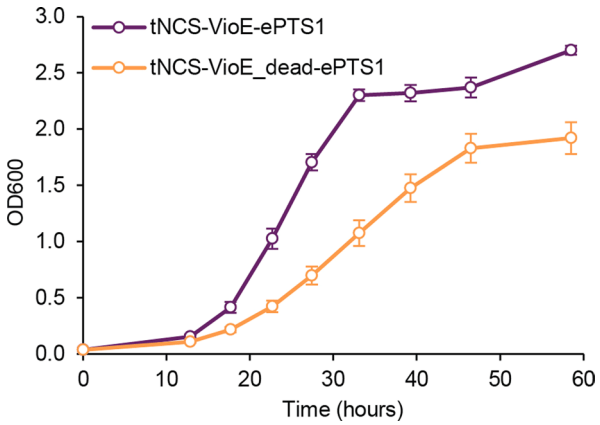

Extended Data Fig. 5 | OD data from 2μ (*S*)-norcoclaurine shake flask fermentation experiment. tNCS-VioE-ePTS1 and -dead_ePTS1 constructs were expressed using the strong pTDH3 promoter on a 2μ plasmid. Error bars represent mean ± s.d. of four biological replicates.

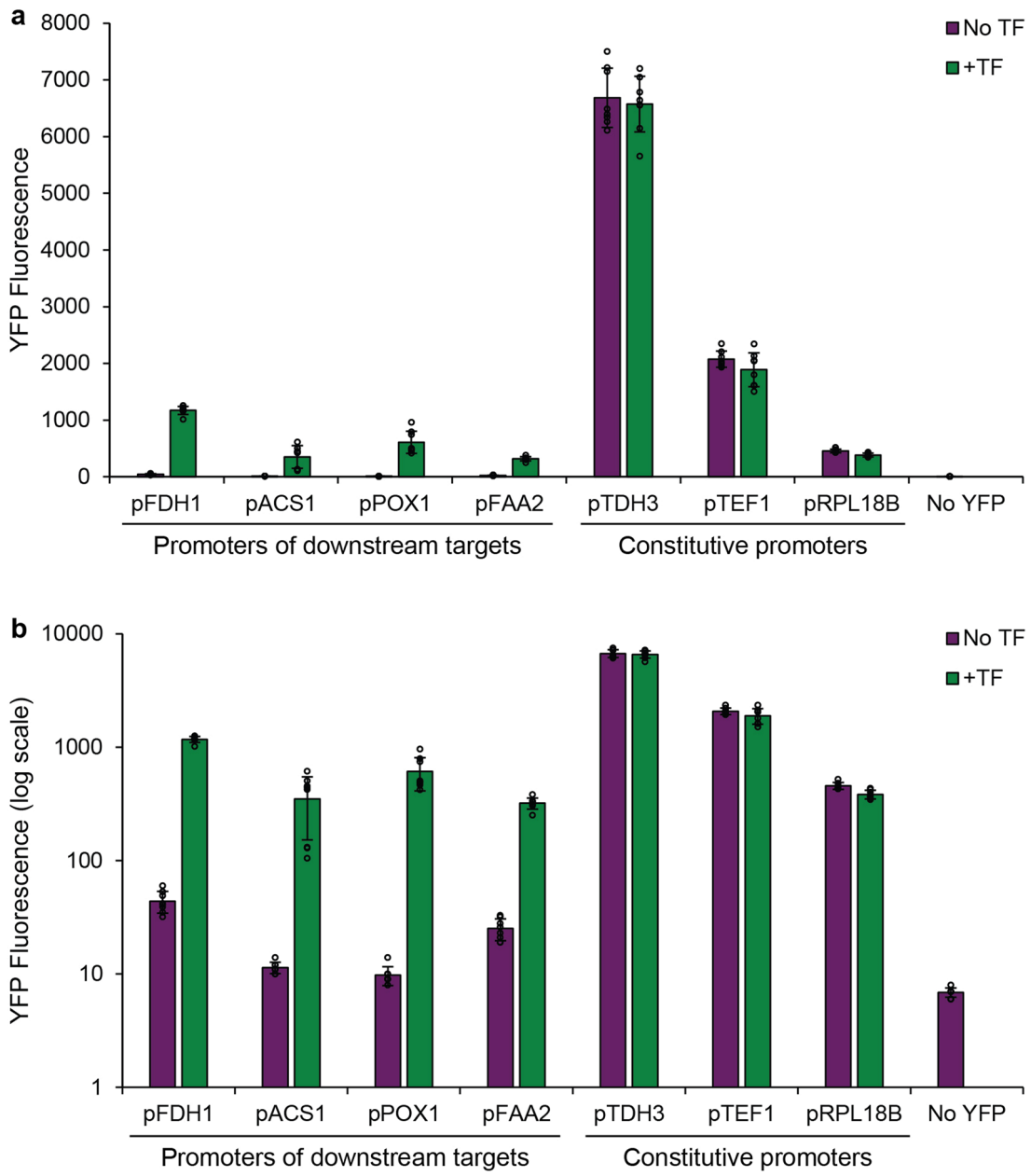

Extended Data Fig. 6 | Expression of engineered transcription factors activates promoters in the peroxisome proliferation network. Promoters were used to drive expression of yellow fluorescent protein (YFP). Promoters pFDH1 and pACS1 are targets of the ADR1 transcription factor, pFAA2 is a target of the OAF1/PIP2 transcription factors, and pPOX1 is a target of both transcription factor types[37,38]. Promoters pTDH3, pTEF1, and pRPL18B are previously characterized constitutive promoters[23]. In addition to YFP, strains contained either a LEU2 marker only (No TF) or ADR1c, OAF1c, and PIP2c, plus a LEU2 marker (+TF). Error bars represent mean ± s.d. of eight biological replicates. **a**, Linear scale. **b**, Log scale.

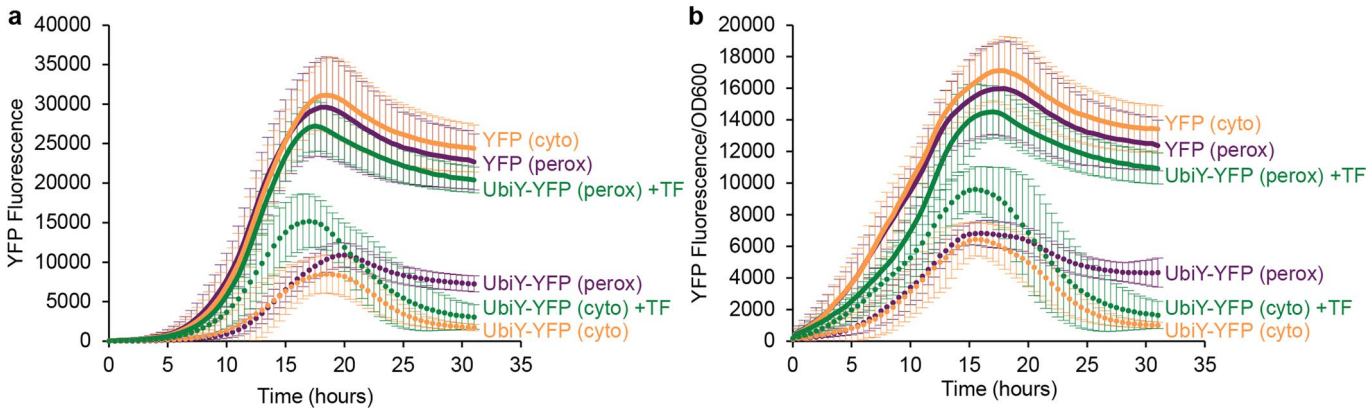

Extended Data Fig. 7 | Dynamics of peroxisomal protection of UbiY-YFP-ePTS1 from degradation. a, Fluorescence. **b**, Fluorescence normalized by OD600. Yellow fluorescent protein (YFP) was expressed with an N-terminal degradation signal (UbiY) in the presence or absence of constitutively-active transcription factors ADR1c/OAF1c/PIP2c (+TF). All strains contain the peroxisomal targeting signal ePTS1 fused to YFP. Constructs transformed into a wildtype background strain will target (UbiY-)YFP-ePTS1 protein to the peroxisome (perox). Cytosolic expression of (UbiY-)YFP-ePTS1 (cyto) is achieved by use of a *pex5*Δ background strain, which is import-deficient due to knockout of the cytosolic receptor protein Pex5p. Error bars represent mean ± s.d. of twelve biological replicates.

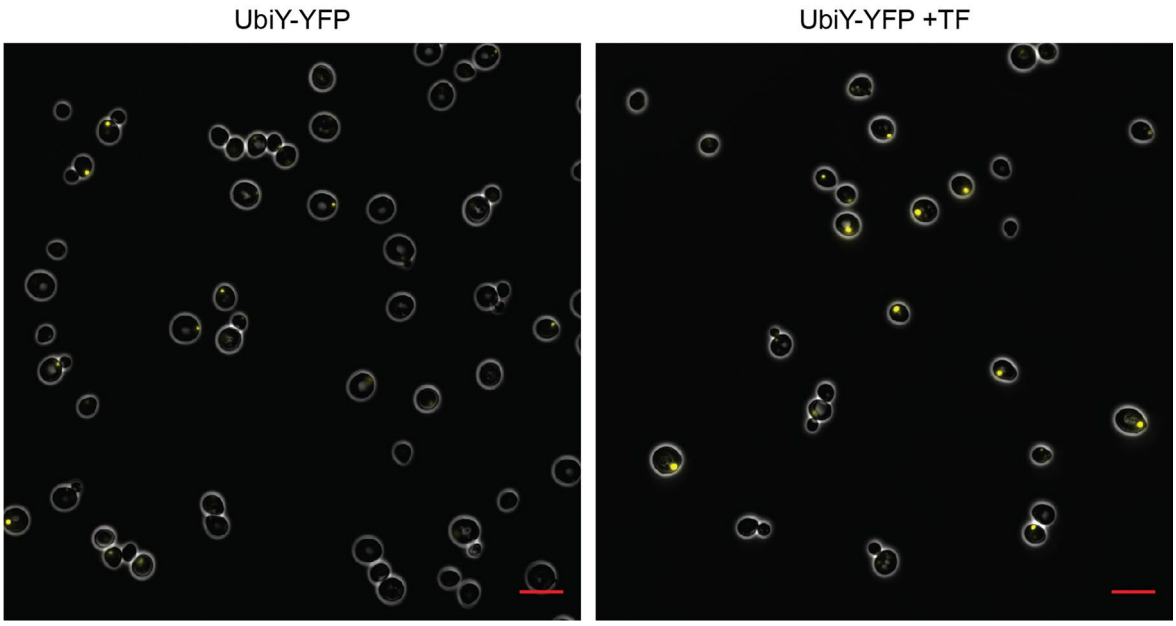

Extended Data Fig. 8 | Expression of engineered transcription factors increases protection of peroxisomally-targeted UbiY-YFP-ePTS1 (zoomed-out version of Fig. 4c). Fluorescence microscopy showing cells without (left) or with (right) expression of constitutively-active transcription factors ADR1c, OAF1c, PIP2c (+TF). Both strains contain YFP fused to the UbiY degradation signal on the N-terminus and the peroxisomal targeting signal ePTS1 on the C-terminus. YFP channel brightness was increased identically across both images to allow better visualization of peroxisomes from the UbiY-YFP strain. Scale bars = 50 μm. Experiment was repeated four times with similar results.

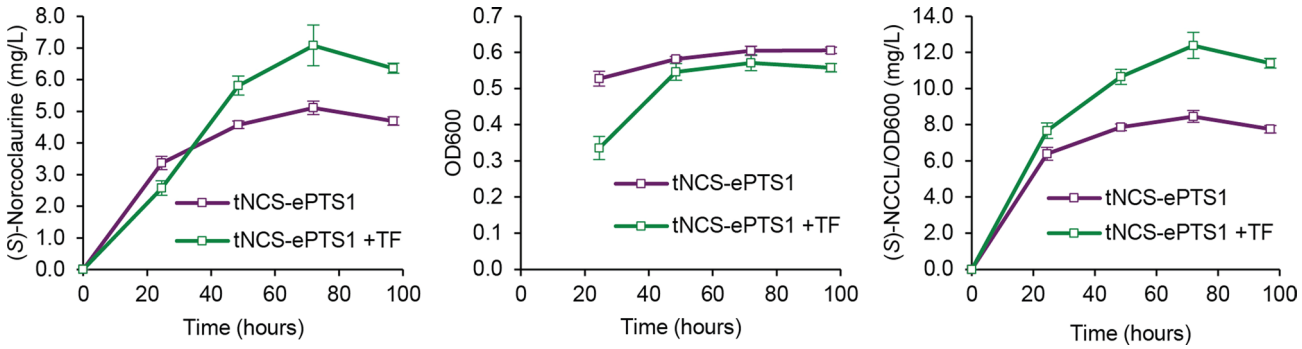

Extended Data Fig. 9 | (*S*)-Norcoclaurine titer, OD600, and OD-normalized titer from transcription factor overexpression experiment. All strains contain the upstream BIA pathway plus 2μ pTDH3-tNCS-ePTS1. The +TF strain also contains ADR1c, OAF1c, and PIP2c. Error bars represent mean ± s.d. of eight biological replicates.

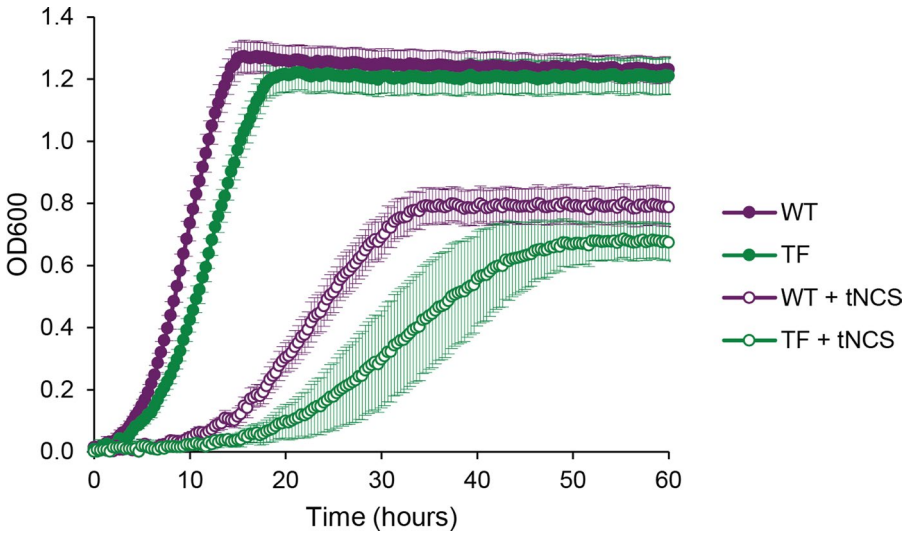

Extended Data Fig. 10 | Expression of engineered transcription factors is linked to slower growth. All strains contain the upstream BIA pathway. Strains without transcription factor overexpression (WT) contain a LEU2 marker. Strains with transcription factor overexpression (TF) contain ADR1c, OAF1c, PIP2c, and a LEU2 marker. Error bars represent mean ± s.d. of twelve biological replicates.

nature research

Corresponding author(s): John Dueber

Last updated by author(s): Aug 2, 2020

Reporting Summary

Nature Research wishes to improve the reproducibility of the work that we publish. This form provides structure for consistency and transparency in reporting. For further information on Nature Research policies, see our Editorial Policies and the Editorial Policy Checklist.

Statistics

For all statistical analyses, confirm that the following items are present in the figure legend, table legend, main text, or Methods section.

n/a	Confirmed	
☐	☒	The exact sample size (*n*) for each experimental group/condition, given as a discrete number and unit of measurement
☐	☒	A statement on whether measurements were taken from distinct samples or whether the same sample was measured repeatedly
☒	☐	The statistical test(s) used AND whether they are one- or two-sided *Only common tests should be described solely by name; describe more complex techniques in the Methods section.*
☒	☐	A description of all covariates tested
☒	☐	A description of any assumptions or corrections, such as tests of normality and adjustment for multiple comparisons
☐	☒	A full description of the statistical parameters including central tendency (e.g. means) or other basic estimates (e.g. regression coefficient) AND variation (e.g. standard deviation) or associated estimates of uncertainty (e.g. confidence intervals)
☒	☐	For null hypothesis testing, the test statistic (e.g. *F*, *t*, *r*) with confidence intervals, effect sizes, degrees of freedom and *P* value noted *Give P values as exact values whenever suitable.*
☒	☐	For Bayesian analysis, information on the choice of priors and Markov chain Monte Carlo settings
☒	☐	For hierarchical and complex designs, identification of the appropriate level for tests and full reporting of outcomes
☒	☐	Estimates of effect sizes (e.g. Cohen's *d*, Pearson's *r*), indicating how they were calculated

Our web collection on statistics for biologists contains articles on many of the points above.

Software and code

Policy information about availability of computer code

Data collection	The following commercial software was used for data collection: SparkControl V2.3, Spark Control V1.2.20, i-control 1.10 for Tecan plate readers; ZEN 2.6 (blue edition) for Zeiss microscope; Agilent Chem Station B.03.04-SP1 for LC/MS.
Data analysis	The following commercial software was used for data analysis: ZEN 3.0 (blue edition) for microscopy data; Microsoft Excel 2013.

For manuscripts utilizing custom algorithms or software that are central to the research but not yet described in published literature, software must be made available to editors and reviewers. We strongly encourage code deposition in a community repository (e.g. GitHub). See the Nature Research guidelines for submitting code & software for further information.

Data

Policy information about availability of data

All manuscripts must include a data availability statement. This statement should provide the following information, where applicable:

- Accession codes, unique identifiers, or web links for publicly available datasets
- A list of figures that have associated raw data
- A description of any restrictions on data availability

The datasets generated and analyzed during the current study are available from the corresponding author on reasonable request. Plasmids are available through Addgene under deposit number 78460.

Field-specific reporting

Please select the one below that is the best fit for your research. If you are not sure, read the appropriate sections before making your selection.

☒ Life sciences ☐ Behavioural & social sciences ☐ Ecological, evolutionary & environmental sciences

For a reference copy of the document with all sections, see nature.com/documents/nr-reporting-summary-flat.pdf

Life sciences study design

All studies must disclose on these points even when the disclosure is negative.

Sample size	All sample sizes were at least n=3 biological replicates, which is standard in our field (e.g. Meadows, A. L. et al. Rewriting yeast central carbon metabolism for industrial isoprenoid production. Nature 537, 694–697 (2016); Galanie, S., Thodey, K., Trenchard, I. J., Interrante, M. F. & Smolke, C. D. Complete biosynthesis of opioids in yeast. Science 349, 1095–1100 (2015)) and was deemed sufficient because major differences between biological replicates were not observed. Sample sizes are reported in each figure legend.
Data exclusions	No data were excluded from the analyses.
Replication	All experiments were performed at least two times, on different days, to verify reproducibility. All attempts at replication were successful.
Randomization	Randomization was not performed because genetically identical samples were used (e.g. biological replicates from a transformation plate).
Blinding	Investigators were unblinded during data collection and analysis due to the quantitative and non-subjective nature of the analyses.

Reporting for specific materials, systems and methods

We require information from authors about some types of materials, experimental systems and methods used in many studies. Here, indicate whether each material, system or method listed is relevant to your study. If you are not sure if a list item applies to your research, read the appropriate section before selecting a response.

Materials & experimental systems

n/a	Involved in the study
☒	☐ Antibodies
☐	☒ Eukaryotic cell lines
☒	☐ Palaeontology and archaeology
☒	☐ Animals and other organisms
☒	☐ Human research participants
☒	☐ Clinical data
☒	☐ Dual use research of concern

Methods

n/a	Involved in the study
☒	☐ ChIP-seq
☒	☐ Flow cytometry
☒	☐ MRI-based neuroimaging

Eukaryotic cell lines

Policy information about cell lines

Cell line source(s)	The base Saccharomyces cerevisiae strain for all experiments was BY4741. Base strain BY4741 and BY4741 pex5Δ were ordered from Open Biosystems—GE Dharmacon.
Authentication	Saccharomyces cerevisiae strains were obtained from Open Biosystems—GE Dharmacon. No further authentication was performed.
Mycoplasma contamination	Saccharomyces cerevisiae strains were not tested for mycoplasma contamination.
Commonly misidentified lines (See ICLAC register)	No commonly misidentified cell lines were used in this study.